Signatures of autoionization in the angular electron distribution in two-photon double ionization of Ar

S. Augustin,[1] M. Schulz,[2] G. Schmid,[1] K. Schnorr,[1] E. V. Gryzlova,[3] H. Lindenblatt,[1] S. Meister,[1] Y. F. Liu,[1] F. Trost,[1] L. Fechner,[1] A. N. Grum-Grzhimailo,[3] S. M. Burkov,[4] M. Braune,[5] R. Treusch,[5] M. Gisselbrecht,[6] C. D. Schröter,[1] T. Pfeifer,[1] and R. Moshammer[1]

[1]*Max-Planck-Institut für Kernphysik, Saupfercheckweg 1, 69117 Heidelberg, Germany*
[2]*Physics Department and LAMOR, Missouri University of Science and Technology, Rolla, Missouri 65409, USA*
[3]*Skobeltsyn Institute of Nuclear Physics, Lomonosov Moscow State University, Moscow, 119991 Russia*
[4]*Pacific National University, Tihookeanskaya Strasse 139, Khabarovsk 680035, Russia*
[5]*DESY, Notkestrasse 85, 22607 Hamburg, Germany*
[6]*Lund University, Sölvegatan 14A, Lund, Sweden*

(Received 23 July 2018; published 17 September 2018)

A kinematically complete experiment on two-photon double ionization of Ar by free-electron laser radiation with a photon energy of 27.93 eV was performed. The electron energy spectra show that double ionization is dominated by the sequential process. Comparison of the electron angular distributions to our data for single ionization and to theory confirms that even in the sequential process the electrons from both ionization steps are correlated with each other through polarization of the intermediate Ar^+ state. Furthermore, a very important role of autoionization in both ionization steps is found.

DOI: 10.1103/PhysRevA.98.033408

I. INTRODUCTION

Until about 10 to 20 years ago experimental studies of nonlinear interactions between light and matter were limited to the relatively small photon energies of optical lasers. Synchrotron radiation has been used for a long time to study photon-atom interactions for photon energies as large as keV's [1]. However, the achievable intensities are smaller by orders of magnitudes compared to conventional lasers so that nonlinear effects are insignificant. For such large photon energies and small intensities transitions in the target atom are predominantly induced by the absorption of a single photon. One process that has been studied extensively is double ionization of the target, which for single photon absorption can only occur in the presence of strong electron-electron correlations [2–5]. With the development of free-electron lasers (FELs) [6] photon intensities comparable to conventional lasers are now available in the extreme ultraviolet and vacuum ultraviolet regime. At sufficiently large intensities two-photon double ionization (TPDI) can dominate over double ionization by single-photon absorption even when the latter is energetically possible [7].

Two different TPDI channels can be distinguished: in one, dubbed direct double ionization (DDI), two photons are absorbed simultaneously, leading to a doubly ionized final state through a virtual intermediate state. This process relies on correlation between the two active electrons. DDI has a threshold energy which is equal to half the double-ionization potential $I^{2+} = I^o + I^+$ of the target atom. The second channel, called sequential double ionization (SDI), can be viewed as two successive (and to a large extent independent) single ionization events: the absorption of one photon leads to the formation of a real intermediate state of the singly charged ion which then absorbs a second photon, resulting in a doubly charged ion. The threshold energy for SDI is equal to the ionization potential of the singly charged ion I^+, which is larger than $1/2 I^{2+}$. Therefore, for photon energies between $1/2 I^{2+}$ and I^+ TPDI is only possible through the correlated DDI process. In this energy regime double ionization by three-photon absorption has also been observed [8]. In contrast, for photon energies larger than I^+ TPDI is dominated by SDI [7].

At first glance, one might expect that in SDI the two ionization steps are completely independent of each other. This would imply that the first electron ejected in double ionization behaves exactly like the electron ejected in single ionization of the neutral target atom and the second electron behaves like the electron ejected in single ionization of a singly charged, unpolarized target ion. For example, the angular distributions of each of the electrons ejected in double ionization, measured relative to the FEL polarization vector, would then be identical to those of the distributions of electrons ejected in the corresponding single ionization events. The latter is given in terms of the differential cross section by the standard dipole expression as

$$d\sigma_1/d\Omega = \sigma_1/4\pi[1 + \beta_2 p_2(\cos\theta)]. \quad (1)$$

Here, σ_1 is the partial photoionization cross section, P_2 is the second Legendre polynomial, and β_2 is the so-called asymmetry parameter, which is a measure of the final-state target anisotropy and is expressed in terms of photoionization amplitudes. However, it was pointed out that even in SDI the two electrons are not completely uncorrelated [9] and that Eq. (1) does not hold for the two ionization steps in SDI. The reason is that Eq. (1) only holds for an unpolarized initial target state, but the first ionization step in SDI generally

leaves the intermediate singly charged target state polarized, i.e., its magnetic substates are not populated uniformly. For example, the ground state of Ar^+, the $3p^5 {}^2P_{3/2}$ state, has substates with $M_J = \pm 1/2$ and $\pm 3/2$, but the ionization cross sections for $|M_J| = 1/2$ and $3/2$ are not the same. It is not surprising that this polarization modifies the angular distribution of the second ejected electron. However, if both electrons are detected in a coincidence experiment, even when the second electron signal is integrated over all angles, the detection of the latter has a feedback effect on the first electron and its angular distribution is also modified as a result of entanglement between the first electron and the singly charged ion [9]. To illustrate this point let us consider an extreme scenario. Imagine that ionization of Ar^+ is only possible if the initial vacancy is in an $m_j = \pm 3/2$ substate, but single ionization of Ar^0 leads to a uniform population of the $m_j = \pm 1/2$ and $\pm 3/2$ substates. If both electrons ejected in SDI are detected in coincidence only electrons ejected from an $m_j = \pm 3/2$ substate in the first step will be observed because if the electron was ejected from an $m_j = \pm 1/2$ substate the second ionization step could not occur. Therefore, the polarization of the intermediate state of SDI is different from the polarization of the final state in single ionization. The corresponding modification of β_2 merely accounts for the statistical population of the intermediate substates. However, in addition for both electrons ejected in SDI a higher-order Legendre term has to be added in the angular distribution. This term is a direct reflection of entanglement between the first electron and the singly charged ion. The modified angular electron distribution can be expressed as

$$d\sigma_i/d\Omega = \sigma/4\pi[1 + {}^{(i)}\beta_2 P_2(\cos\theta) + {}^{(i)}\beta_4 P_4(\cos\theta)] \quad (2)$$

where the index $i = 1, 2$ refers to the two electrons.

These predictions by theory were tested by several experimental studies [10–14] (for a review see [15]). The angular distribution of the second electron ejected in SDI from the np^6 shells of Ne, Ar, Kr, and Xe was measured for various photon energies by Braune *et al.* [10]. Generally, experiment and theory are in satisfactory agreement, although there are deviations between them in some cases. Furthermore, disagreement among various calculations [9,14,16] based on nonrelativistic and relativistic Hartree-Fock approaches and on the random-phase approximation with exchange exists. The fine-structure $np^5 {}^2P_j$ doublet of the intermediate singly charged ion was considered both coherently and incoherently. To the best of our knowledge only one experiment was performed in which the angular distribution of both electrons was measured in coincidence. There, TPDI of Ne for a photon energy of 44 eV was studied by Kurka *et al.* [11]. Within the experimental uncertainties the ${}^{(2)}\beta$ parameters of both electrons were consistent with theory. However, the difference between the theoretical β parameters for a polarized and unpolarized intermediate singly charged target state was too small to be conclusively observable within the experimental error bars. Also, the ${}^{(2)}\beta_4$ parameters measured in the experiments reported in [10,11] were very different from each other, which was quite surprising considering that there was not a large difference in the photon energies.

In this paper we report on a coincidence experiment and on theoretical calculations on TPDI of Ar by an FEL pulse with a photon energy of 27.93 eV. Small but significant differences between the angular distributions of the first electron in TPDI and of the electron ejected in single ionization were established. Furthermore, the comparison between experiment and theory reveals a very important role of autoionization in each step of TPDI.

II. EXPERIMENT

The experiment was performed at the beamline BL2 of the FEL in Hamburg (FLASH). The setup was very similar to the one described in [17,18]. The FEL beam, with a photon energy of 27.93 ± 0.25 eV, was linearly polarized and pulsed with an effective repetition rate of 600 Hz and a single pulse duration of approximately 50 fs. The bandwidth is not known with high accuracy, which introduces substantial uncertainties which should be kept in mind when comparing experiment with theory. The averaged peak intensity was about 3×10^{13} W/cm^2 with an uncertainty of $\pm 2 \times 10^{13}$ W/cm^2. The beam was focused to a size of about 25 μm in diameter and crossed with a collimated neutral Ar beam from a supersonic jet with the intersection point of both beams located at the focal point. The propagation direction of the target beam was parallel to the polarization of the FEL beam.

The ejected electrons and the recoil ions were momentum-analyzed with a reaction microscope (ReMi) [19] located in an ultra-high-vacuum chamber with a base pressure of $\sim 10^{-11}$ mbar. Uniform weak electric and magnetic fields of 1.52 V/cm and 8.2 G were applied to extract the electrons and recoil ions in opposite directions along an axis perpendicular to both the photon and target beam directions to guide them onto time- and two-dimensional position-sensitive multichannel plate detectors. The recoil-ion detector, with a size of 110 mm in active diameter, consisted of two channel plates (chevron stack) and a delay-line anode with two pairs of wires (quadanode). The electron detector consisted of three channel plates (z stack) and a delay-line anode with three pairs of wires (hexanode). Both detectors were multihit capable so that two electrons ejected in the same double ionization event could be detected and momentum-analyzed. Although only one recoil ion is generated for each ionization event the multihit capability is nevertheless crucially important because of the large instantaneous recoil-ion detection rate due to the intense photon beam. Without multihit capability there would be a very large probability that a false recoil ion (i.e., one resulting from a different ionization event than the electrons), but not the true recoil ion, would be detected. Both detectors were set in coincidence.

The electric field was large enough to reverse the direction of electrons with an energy of up to 22 eV initially ejected away from the detector. The magnetic field forced the electrons into cyclotron orbits. For electron momenta perpendicular to the electric field of up to 1.35 a.u. (corresponding to an energy of 25 eV) the cyclotron radius was small enough for the electrons to be guided onto the detector. Therefore, all electrons with energies smaller than 22 eV and practically all recoil ions (because their kinetic energy was less than 200 μeV) were detected with 4π solid angle. From the position and time-of-flight information, contained in the coincidence times, all three momentum components of each detected

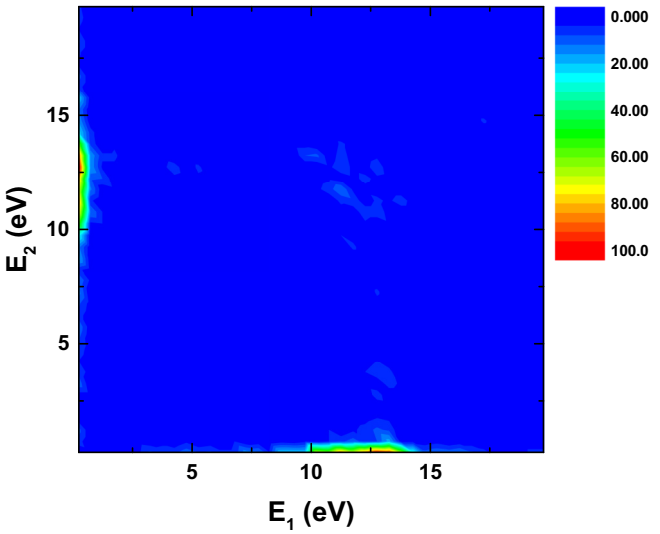

FIG. 1. Two-dimensional energy spectrum of two electrons measured in coincidence in TPDI of Ar.

particle were deduced. The electron energy resolution depends on the energy itself and is estimated to be about 0.02-eV full width at half maximum (FWHM) for the slow (second) electron and about 0.8-eV FWHM for the fast (first) electron.

III. RESULTS AND DISCUSSION

The threshold energies for DDI and sequential TPDI are 21.7 and 27.63 eV [20], respectively, so that both are energetically possible for the photon energy used in this experiment. However, the coincident two-dimensional energy spectrum of both electrons, plotted in Fig. 1, demonstrates that TPDI is completely dominated by SDI. The signature of SDI is an electron energy combination of $E_f = E_\gamma - I^o \approx 12.2\,\mathrm{eV}$ and $E_s \approx E_\gamma - I^+ \approx 0.3\,\mathrm{eV}$ (where E_γ is the photon energy and the subscripts stand for fast and slow, respectively), both broadened by the energy spread in the FEL beam (the energy spectrum of the fast electron is further broadened by the experimental resolution). Indeed, the two main structures are found exactly at these energy combinations. The signature of DDI, on the other hand, is $E_f + E_s = 2E_\gamma - (I^o + I^+) \approx 12.5\,\mathrm{eV}$, i.e., the diagonal line connecting the two maxima representing DSI. Virtually no intensity is found along this line illustrating that DDI is essentially absent. A very weak maximum is found for $E_1 = E_2 \approx 12\,\mathrm{eV}$ (where E_1 and E_2 are the two detected electron energies), which is due to false coincidences between two single ionization events of two different Ar atoms.

Angular distributions of both ejected electrons were analyzed with a condition on the main maxima in Fig. 1 thus cleaning the SDI contributions from any background due to separate single ionization events. The angular distribution of the electron ejected in the first ionization step, measured relative to the polarization vector of the FEL light, is plotted in the left panel of Fig. 2, where the final states of the Ar^+ ion (i.e., the intermediate states of the TPDI process) could not be resolved. For comparison, the center panel shows the angular distribution for single ionization measured in coincidence with Ar^+ ions. It should be noted that for the fast electron ejected at angles smaller than -45° and larger than 45° it has completed nearly one cycle of the cyclotron motion generated by the magnetic field of the ReMi. In this region the electron momentum resolution is poor so that information about the ejection angle can only be obtained in the range from -45 to 45°. Both angular distributions appear to be very similar and this is supported by fits of Eq. (2) to the measured spectra shown as black dashed curves. For single ionization this fit yields $\beta_2 = 1.4 \pm 0.035$ and $\beta_4 = -0.024 \pm 0.035$, which is consistent with the expectation that β_4 should be exactly zero for single ionization. Furthermore, these values agree very well both with theory [21] and experimental data [22,23]. For the first step of double ionization the fit yields ${}^{(1)}\beta_2 = 1.39 \pm 0.1$ and ${}^{(1)}\beta_4 = 0.13 \pm 0.11$.

Within experimental uncertainties β_2 is identical for the fast electron in SDI and single ionization. For β_4 a small difference is found, which is barely outside the error bars. The confidence level that this difference is real is less than 70% and the data cannot be regarded as conclusive in this regard. However, more significant results are obtained from the analysis of the ratios R between the angular distributions of both cases, which are shown in the right panel of Fig. 2. Since both angular distributions are recorded simultaneously under identical experimental conditions systematic uncertainties cancel to a large extent in these ratios. The data reveal a pronounced peak structure at about 90° and R becomes smaller than 1 on both sides of the maximum. All data points except for one depart from $R = 1$ within the statistical error bars. Furthermore, the ratio between the fits of Eq. (2) to the angular distributions (black dashed curve) agrees very well with the measured ratios. The structure in R is mainly caused by the difference in β_4; the effect due to the very small difference in β_2 would barely be visible in the plots of Fig. 2.

The blue dashed curves show our calculations, averaged over all Ar^+ states as described in [9,21]. The theoretical description is based on the standard statistical tensor and density matrix of angular momentum formalism [24]. This approach separates geometrical and dynamical parts in the equations describing the process, with only the latter part depending on the photoionization amplitudes. These amplitudes were calculated within first-order perturbation theory in the dipole approximation by the multiconfiguration Hartree-Fock (MCHF) approximation [25]. In the MCHF description of the ground-state wave function, we mixed the configurations $3p^m + 3p^{m-1}4s + 3p^{m-1}3d + 3p^{m-2}3d^2 + 3p^{m-2}4s3d + 3p^{m-2}4s^2$, where $m = 6$ for the neutral atom and $m = 5$ for the singly charged ion. The Hartree-Fock term-dependent $3p^m E, l$ continuum wave functions with the frozen $3p^m$ core were used for describing the final state, where E and l are the energy and orbital angular momentum of the photoelectron, respectively. The MCHF calculation yields ${}^{(1)}\beta_2 = 1.45$ and ${}^{(1)}\beta_4 = -0.08$ for the fast electron ejected in SDI and $\beta_2 = 1.35$ for single ionization. Although the differences between these theoretical parameters and those obtained from the fit to the experimental data are rather small, they nevertheless lead to some visible discrepancies in the angular distributions. The experimental ratios, on the other hand, are not even qualitatively reproduced by theory, which shows a pronounced minimum at 90°, where

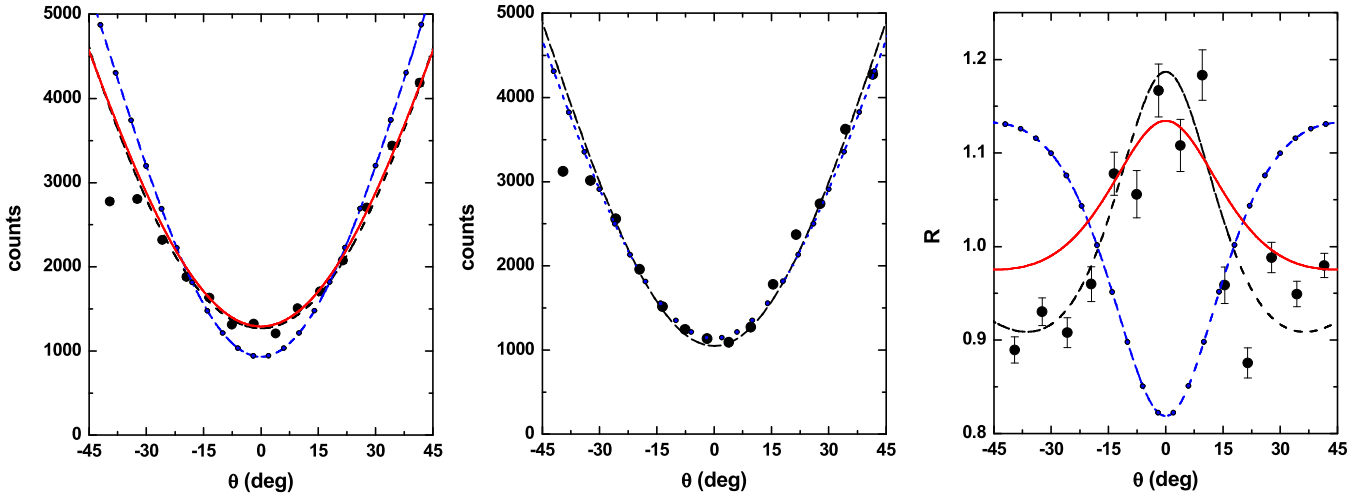

FIG. 2. Angular distribution of the fast electron ejected in the first step of TPDI (left panel) and of the electron ejected in single ionization (center panel). The right panel shows the ratio between both angular distributions. Black dashed curves, fit of Eq. (2) to the data; blue dashed curves, calculations not accounting for autoionization; red solid curves, calculations accounting for autoionization.

the measured ratios have a maximum. While theory and experiment agree that even the first electron in SDI is affected by the polarization of the intermediate state, they do not agree on how it is affected.

In the left panel of Fig. 3 we present the angular distribution of the second electron ejected in SDI averaged over all electron energies between 0 and 1 eV. For such very small energies the electrons only complete a small fraction of one cyclotron cycle so that here we obtained angular information with sufficient resolution over the entire range from -90 to 90°. At first glance, the angular distribution of the slow electron looks quite similar to the one of the first electron. However, a fit of Eq. (2) to the measured spectrum (black dashed curves in Fig. 3) yields a substantially smaller ${}^{(2)}\beta_2$ parameter (${}^{(2)}\beta_2 = 0.82 \pm 0.053$) for the slow electron, while the ${}^{(2)}\beta_4$ parameter (${}^{(2)}\beta_4 = 0.06 \pm 0.07$) has, within experimental uncertainties, the same value as for the fast electron. The blue dashed curve in the left panel of Fig. 3 shows our calculation for the second electron averaged over all Ar^{2+} states, which yields ${}^{(2)}\beta_2 = 1.3$ and ${}^{(2)}\beta_4 = -0.06$. As expected, the change of the β parameters relative to those for an unpolarized intermediate state is larger than for the first electron. However, the theoretical ${}^{(2)}\beta_2$ parameter is in poor agreement with the experimental value.

The magnitude of the discrepancies between the experimental and theoretical value of ${}^{(2)}\beta_2$, as well as the poor agreement in the ratio between the angular distributions of the first electron and single ionization (Fig. 2), suggest that something qualitatively important may be missing in our theoretical model. One aspect which is not accounted for at all in the MCHF calculation is transitions of the electron to the continuum through autoionizing intermediate states. For example, instead of directly lifting the first electron to the continuum, the absorption of the first photon can lead to a transition to the $3s3p^6 5p\,{}^1\mathrm{P}_1$ state. This is a particle-hole state with an energy (27.997 eV [20]) larger than the ground state

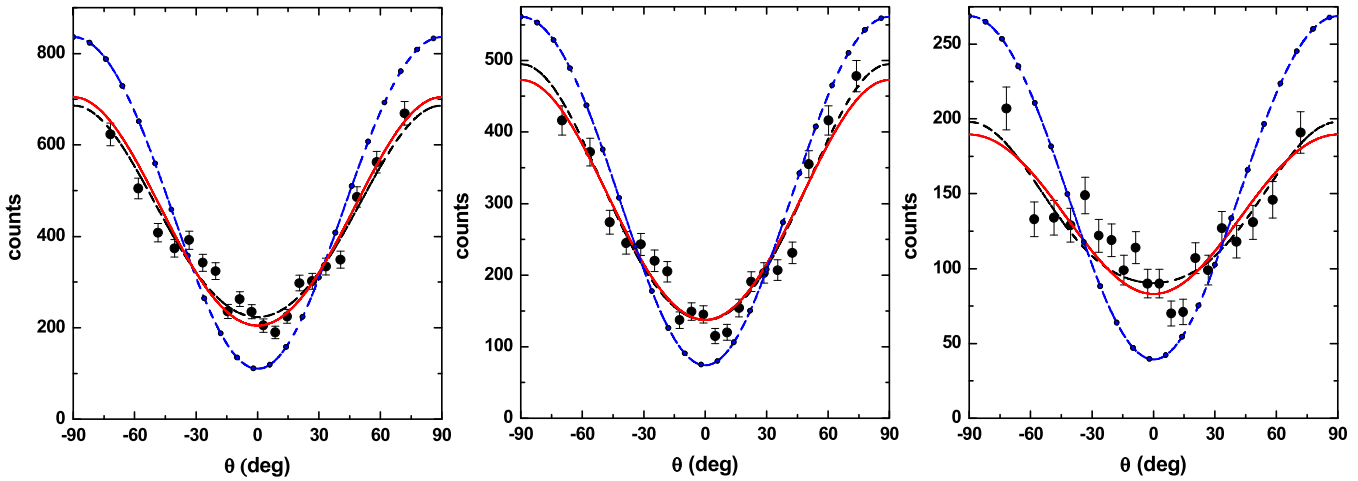

FIG. 3. Angular distribution of the slow electrons ejected in the second step of sequential two-photon double ionization averaged over all energies smaller than 1 eV (left panel). The center and right panels show the same angular distributions averaged over the energy intervals 0.2 to 0.4 eV and 0.4 to 0.6 eV, respectively. Curves: same as in Fig. 2.

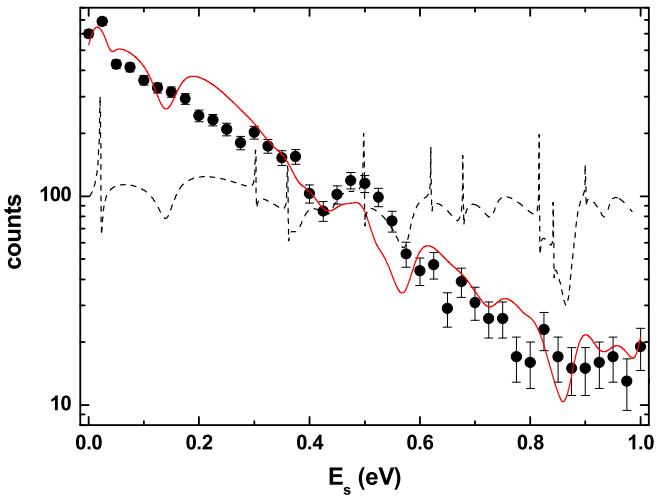

FIG. 4. Energy spectrum of the slow electron ejected in the second step of sequential TPDI. The black dashed curve shows the calculated energy spectrum not accounting for the FEL spectral profile or the electron energy resolution. The red solid curve represents the same calculation multiplied by the spectral profile and convoluted with the electron energy resolution.

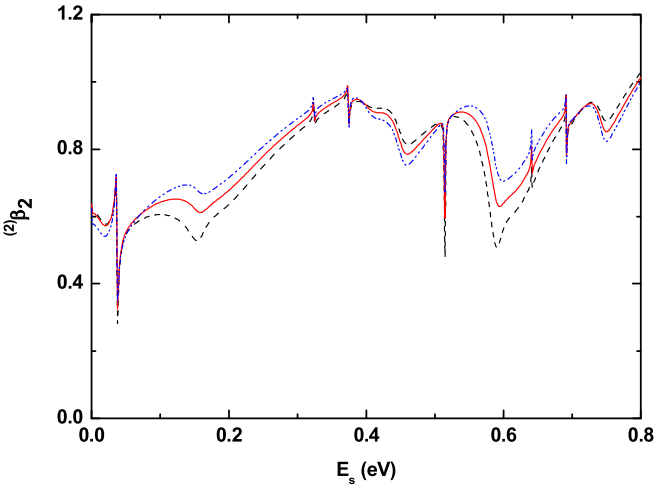

FIG. 5. Electron energy dependence of the $^{(2)}\beta_2$ parameter for the electron ejected in the second step of sequential two-photon double ionization calculated with autoionization included for three different photon energies within the FEL bandwidth.

of Ar^+ and it can therefore autoionize to the $3s^2 3p^5\,{}^2P_{1/2}$ or $3s^2 3p^5\,{}^2P_{3/2}$ states. The excitation energy of the $3s3p^6 5p\,{}^1P_1$ state is accessible within the FEL bandwidth of approximately ± 0.25 eV. For the second electron a multitude of Rydberg autoionizing states can contribute to the ionization of the intermediate Ar^+ ion. Such autoionizing states are known to crucially influence the angular distributions of photoelectrons in single ionization of neutral atoms by synchrotron radiation (see, e.g., [26–28]).

The energy spectrum of the second (slow) electron, plotted in Fig. 4, confirms that autoionization resonances can play an important role. The black dashed curve shows the theoretical energy spectrum incorporating the autoionizing states within the R-matrix approach (which is one standard method of incorporating autoionizing states in the theoretical treatment of photoionization) [29,30] and without accounting for the FEL bandwidth and the electron energy resolution. We performed the nonrelativistic R-matrix calculations independently for the first and the second ionization steps, the latter accounting for the alignment of the intermediate ionic state. In the calculations of the first step the states $(3p^5\,{}^2P)$, $(3s3p^6\,{}^2S)$, $[3p^4({}^3P)4s^2P]$, $[3p^4({}^3P)3d^2P, {}^2D, {}^2F]$, and $[3p^4({}^1D)3d^2D]$ of Ar^+ were used and for the second step the states $(3s^2 3p^4\,{}^3P, {}^1D, {}^1S)$ and $(3s3p^5\,{}^1P, {}^3P)$ of Ar^{2+} were used. The fine structure of the residual ion was taken into account by using statistical weights of the fine-structure levels, defined by their angular momentum, and shifting the theoretical curves in accordance with experimental values of the energy splitting [20]. Six series of autoionizing states lie energetically between the $Ar^{2+}\ 3p^4\,{}^3P$ and $3p^4\,{}^1D$ thresholds and can be excited by photoabsoption from the $Ar^+\ 3p^5\,{}^2P$ state: $(3p^4\,{}^1D$ nd $^2D)$, $(3p^4\,{}^1D$ nd $^2P)$, $({}^1D$ nd $^2S)$, $(3p^4\,{}^1D$ ns $^2D)$, $(3p^4\,{}^1S$ nd $^2D)$, and $(3p^4\,{}^1S$ ns $^2S)$. However, only the first two series of this list, each for $n = 6, 7, 8$, affect the energy spectrum of the slow electron in the region of interest. The ^2D resonances are sharp and only decay by emission of d-wave electrons, while the ^2P resonances are broad and decay by emission of both, s and d waves.

The resonance energies in this calculation are consistent with photoionization spectra of Ar^+ measured and calculated in the Breit-Pauli R-matrix approximation by Covington *et al.* [31]. These predicted resonances seem to coincide with corresponding structures in the experimental spectrum, most notably at an electron energy of 0.51 eV. The solid red curve shows the calculation multiplied by the spectral profile of the FEL beam, using a bandwidth of ± 0.22 eV, and convoluted with an electron energy resolution of 0.018-eV FWHM, which is in reasonably good agreement with the experimental spectrum. The values used for the FEL bandwidth and the electron energy resolution are slightly smaller than the estimated numbers provided in the experimental section. However, they yield the best agreement with the measured energy spectrum and are well within the uncertainties of these estimated values.

In Fig. 5 we show $^{(2)}\beta_2$ calculated with the autoionization resonances included as a function of the energy of the second electron. The three curves represent different photon energies within the FEL bandwidth (27.6 eV, black dashed curve; 27.9, red solid curve; and 28.2 eV, blue dash-dotted curve). The sharp structures in these plots illustrate the high sensitivity of $^{(2)}\beta_2$ on the energy of the second electron, while without accounting for autoionization the energy dependence of $^{(2)}\beta_2$ is rather smooth [9,21]. Furthermore, significant variations between different photon energies are found. Since the experimental electron energy resolution and the spread in the photon energy are significantly larger than the width of some of the structures in the theoretical $^{(2)}\beta_2$ the calculations have to be multiplied by the FEL spectral profile and convoluted with the experimental electron energy resolution.

The red solid curves in Figs. 2 and 3 show the theoretical calculations with autoionization resonances included. At first glance the changes in the β parameters of the first electron

($^{(1)}\beta_2 = 1.3$ and $^{(1)}\beta_4 = 0.05$) introduced by the inclusion of autoionization may not appear particularly significant. However, in the ratios between the angular distributions of the first electron in SDI and the electron in single ionization considerably improved agreement with the experimental data is obtained. The minimum obtained when auto-ionization is not included is now turned into a maximum, in accord with the experimental data.

At present, we cannot offer a conceptual explanation for this switch from a minimum to a maximum. However, some additional comments on the formalism might be helpful. Let us assume that a specific channel with fixed orbital angular momentum $L(L = 1, 2)$ of the final Ar^{++} state [e.g., $(3p^4\,{}^3P) + e^-(\varepsilon s,\ \varepsilon d)$ dominates [note that $L = 0$ is forbidden in the LS-coupling approximation for the final $Ar^{++}(3p^4\,{}^3P)$ state]. Furthermore, we assume that the partial cross section for the first ionization step [$Ar(3p^6) \rightarrow Ar^+(3p^5) + e^-(\varepsilon s$ or $ed)$] leading to d-wave photoelectron emission is much larger than for s-wave emission. This is fulfilled very well for our photon energy [32]. Then the procedure described in [33] leads to $^{(1)}\beta_4$ which for fixed L are just constants: $^{(1)}\beta_4^{L=1} = -\frac{108}{203}$ and $^{(1)}\beta_4^{L=2} = +\frac{108}{1057}$, where the right superscript indicates the dominant L channel. While numerical MCHF calculations without accounting for resonances and with all channels included give negative value for $^{(1)}\beta_4$, the R-matrix calculations accounting for strong autoionizing D resonances change the sign of $^{(1)}\beta_4$, which brings $^{(1)}\beta_4$ in agreement with experiment.

For the second electron the inclusion of autoionization has an even larger impact than for the first electron, especially on $^{(2)}\beta_2$, which is now smaller by about 30% ($^{(1)}\beta_2 = 0.9$). In $^{(2)}\beta_4$ the sign is reversed ($^{(2)}\beta_4 = 0.03$), as for the first electron; however, in absolute terms this difference is too small to be experimentally verifiable. These modified β parameters result in excellent agreement between the experimental and theoretical angular distributions of both electrons ejected in SDI (see Fig. 3, left panel).

As mentioned above, the inclusion of autoionization leads to pronounced structures in the electron energy dependence of the β parameters. More specifically, in the energy interval for the slow electron from 0.2 to 0.4 eV the averaged $^{(2)}\beta_2$ parameter is 0.9 and $^{(2)}\beta_4$ is 0.03, while in the interval 0.4 to 0.6 eV it changes to 0.6 and $^{(2)}\beta_4$ changes from 0.03 to -0.02. We have therefore analyzed the experimental angular distributions for these energy intervals, which are shown in the center and right panels of Fig. 3, respectively. From these data, parameters of $^{(2)}\beta_2 = 0.94 \pm 0.06$ and $^{(2)}\beta_4 = 0.08 \pm 0.078$ for 0.2 to 0.4 eV and $^{(2)}\beta_2 = 0.56 \pm 0.075$ and $^{(2)}\beta_4 = 0.09 \pm 0.1$ for 0.4 to 0.6 eV were extracted, in very good agreement with theory.

As a final note we point out that the contributions from autoionization may also be able to explain the discrepancies in $^{(2)}\beta_4$ between the data of Braune *et al.* for Ne [10] and theory not accounting for autoionization [11,16] as well as the differences to the data of Kurka *et al.* [11] for a slightly different photon energy. For SDI of Ar at a photon energy of 27.93 eV $^{(2)}\beta_4$ remains very close to zero when autoionization is included. However, for Ne and a much larger photon energy this could be very different since the β parameters are very sensitive to both the photon energy and the atomic structure.

IV. CONCLUSIONS

In summary, we have performed a coincidence experiment on two-photon double ionization of Ar by free-electron laser radiation for a photon energy of 27.93 eV. As expected, only signatures of sequential double ionization were observed. The measured angular distributions of both photoelectrons were analyzed and compared to calculations. A theoretically predicted correlation between both electrons, resulting from the polarization of the intermediate state of the Ar^+ ion, was confirmed by the experimental data. Furthermore, the comparison between experiment and theory clearly shows the importance of autoionization resonances in both steps of sequential double ionization. This channel might also explain differences between theory and experiment as well as between two different experimental data sets reported earlier for Ne [10,11].

ACKNOWLEDGMENTS

The excellent support by the scientific and technical team at FLASH is gratefully acknowledged. M.S. is supported by the NSF under Grant No. PHY-1703109. K.S. was funded by a Peter Paul Ewald Fellowship from the Volkswagen Foundation. E.V.G. acknowledges financial support from the Basis foundation via the "Junior Leader" program. M.S. and E.V.G. are also grateful for the support and hospitality of the Max-Planck-Institut für Kernphysik in Heidelberg.

[1] V. Schmidt, Z. Phys. D **2**, 275 (1986).
[2] L. Avaldi and A. Huetz, J. Phys. B **38**, S861 (2005).
[3] D. Akoury *et al.*, Science **318**, 949 (2007).
[4] A. Knapp, A. Kheifets, I. Bray, T. Weber, A. L. Landers, S. Schössler, T. Jahnke, J. Nickles, S. Kammer, O. Jagutzki, L. P. Schmidt, T. Osipov, J. Rösch, M. H. Prior, H. Schmidt-Böcking, C. L. Cocke, and R. Dörner, Phys. Rev. Lett. **89**, 033004 (2002)
[5] J. Viefhaus, S. Cvejanovic, B. Langer, T. Lischke, G. Prümper, D. Rolles, A. V. Golovin, A. N. Grum-Grzhimailo, N. M. Kabachnik, and U. Becker, Phys. Rev. Lett. **92**, 083001 (2004).
[6] W. Ackermann *et al.*, Nat. Photonics **1**, 336 (2007).
[7] M. G. Makris and P. Lambropoulos, Phys. Rev. A **77**, 023401 (2008).
[8] H. Fukuzawa, E. V. Gryzlova, K. Motomura, A. Yamada, K. Ueda, A. N. Grum-Grzhimailo, S. I. Strakhova, K. Nagaya, A. Sugishima, Y. Mizoguchi, H. Iwayama, M. Yao, N. Saito, P. Piseri, T. Mazza, M. Devetta, M. Coreno, M. Nagasono, K. Tono, M. Yabashi, T. Ishikawa, H. Ohashi, H. Kimura, T. Togashi, and Y. Senba, J. Phys. B **43**, 111001 (2010).
[9] S. Fritzsche, A. N. Grum-Grzhimailo, E. V. Gryzlova, and N. M. Kabachnik, J. Phys. B **41**, 165601 (2008).
[10] M. Braune, A. Reinköster, J. Viefhaus, B. Lohmann, and U. Becker, HASYLAB Annual Report No. 457, 2007

(unpublished), http://hasyweb.desy.de/science/annual_reports/2007_report/part1/contrib/40/21686.

[11] M. Kurka, A. Rudenko, L. Foucar, K. U. Kühnel, Y. H. Jiang, T. Ergler, T. Havermeier, M. Smolarski, S. Schössler, K. Cole, M. Schöffler, R. Dörner, M. Gensch, S. Düsterer, R. Treusch, S. Fritzsche, A. N. Grum-Grzhimailo, E. V. Gryzlova, N. M. Kabachnik, C. D. Schröter, R. Moshammer, and J. Ullrich, J. Phys. B **42**, 141002 (2009).

[12] G. Hartmann, Coherence effects of diatomic homonuclear molecules and sequential two-photon processes of noble gases in the photoionization, Ph.D. thesis, Technische Universitaet Berlin (University of Technology Berlin), 2014, http://opus4.kobv.de/opus4-tuberlin/frontdoor/index/index/docId/5055.

[13] S. Mondal, R. Ma, K. Motomura, H. Fukuzawa, A. Yamada, K. Nagaya, S. Yase, Y. Mizoguchi, M. Yao, A. Rouzée, A. Hundertmark, M. J. J. Vrakking, P. Johnsson, M. Nagasono, K. Tono, T. Togashi, Y. Senba, H. Ohashi, M. Yabashi, T. Ishikawa, I. P. Sazhina, S. Fritzsche, N. M. Kabachnik, and K. Ueda, J. Phys. B **46**, 164022 (2013).

[14] M. Braune, G. Hartmann, M. Ilchen, A. Knie, T. Lischke, A. Reinköster, A. Meissner, S. Deinert, L. Glaser, O. Al-Dossary, A. Ehresmann, A. S. Kheifets, and J. Viefhaus, J. Mod. Opt. **63**, 324 (2016).

[15] A. N. Grum-Grzhimailo, E. V. Gryzlova, S. Fritzsche, and N. M. Kabachnik, J. Mod. Opt. **63**, 334 (2016).

[16] A. Kheifets, J. Phys. B **40**, F313 (2007).

[17] R. Moshammer, Y. H. Jiang, L. Foucar, A. Rudenko, T. Ergler, C. D. Schröter, S. Lüdemann, K. Zrost, D. Fischer, J. Titze, T. Jahnke, M. Schöffler, T. Weber, R. Dörner, T. J. M. Zouros, A. Dorn, T. Ferger, K. U. Kühnel, S. Düsterer, R. Treusch, P. Radcliffe, E. Plönjes, and J. Ullrich, Phys. Rev. Lett. **98**, 203001 (2007).

[18] A. Rudenko, L. Foucar, M. Kurka, T. Ergler, K. U. Kühnel, Y. H. Jiang, A. Voitkiv, B. Najjari, A. Kheifets, S. Lüdemann, T. Havermeier, M. Smolarski, S. Schössler, K. Cole, M. Schöffler, R. Dörner, S. Düsterer, W. Li, B. Keitel, R. Treusch, M. Gensch, C. D. Schröter, R. Moshammer, and J. Ullrich, Phys. Rev. Lett. **101**, 073003 (2008).

[19] J. Ullrich, R. Moshammer, A. Dorn, R. Dörner, L. Schmidt, and H. Schmidt-Böcking, Rep. Prog. Phys. **66**, 1463 (2003).

[20] *NIST Atomic Spectra Database, version 5.3*, National Institute of Standards and Technology, Gaithersburg, MD, 2015, http://physics.nist.gov/asd.

[21] A. N. Grum-Grzhimailo, E. V. Gryzlova, S. I. Strakhova, N. M. Kabachnik, and S. Fritzsche, J. Phys. Conf. Series **194**, 012004 (2009).

[22] R. G. Houlgate, J. B. West, K. Codling, and G. V. Marr, J. Phys. B **7**, L470 (1974).

[23] M. Y. Adam, P. Morin, and G. Wendin, Phys. Rev. A **31**, 1426 (1985).

[24] V. V. Balashov, A. N. Grum-Grzhimailo, and N. M. Kabachnik, *Polarization and Correlation Phenomena in Atomic Collisions: A Practical Theory Course* (Plenum, New York, 2000).

[25] C. Froese Fischer, T. Brage, and P. Jonsson, *Computational Atomic Structure: An MCHF Approach* (Institute of Physics, Bristol, 1997).

[26] D. R. Cooper, D. Cubric, D. B. Thompson, P. Bolognesi, M. C. A. Lopes, and G. C. King, J. Electr. Spectrosc. Rel. Phemon. **112**, 129 (2000).

[27] D. Dill, Phys. Rev. A **7**, 1976 (1973).

[28] J. A. R. Samson and J. L. Gardner, Phys. Rev. Lett. **31**, 1327 (1973).

[29] P. G. Burke, *R-Matrix Theory of Atomic Collisions. Application to Atomic, Molecular and Optical Processes* (Springer, Berlin, 2011).

[30] K. A. Berrington, W. B. Eissner, and P. H. Norrington, Comp. Phys. Commun. **92**, 290 (1995).

[31] A. M. Covington, A. Aguilar, I. R. Covington, G. Hinojosa, C. A. Shirley, R. A. Phaneuf, I. Álvarez, C. Cisneros, I. Dominguez-Lopez, M. M. Sant'Anna, A. S. Schlachter, C. P. Ballance, and B. M. McLaughlin, Phys. Rev. A **84**, 013413 (2011).

[32] J. R. Swanson and L. Armstrong, Jr., Phys. Rev. A **15**, 661 (1977).

[33] E. V. Gryzlova, A. N. Grum-Grzhimailo, S. Fritzsche, and N. M. Kabachnik, J. Phys. B **43**, 225602 (2010).